Nanosecond laser ablation threshold of liquid tin microdroplets

R. A. Meijer[1,2] · D. Kurilovich[3] · B. Liu[1,2] · Z. Mazzotta[1] · J. Hernandez-Rueda[1] · O. O. Versolato[1,2] · S. Witte[1,2]

Abstract

The laser ablation threshold is an important parameter that governs the response of materials to intense laser irradiation. Here we study the ablation threshold of liquid tin, by irradiating tin microdroplets with nanosecond laser pulses having finely controlled temporal shape and duration. We use the time-dependent reflection from the droplet as the main observable, which exhibits a sharp decrease in magnitude at a given time instance that depends on the laser intensity. This moment marks the generation of a plasma that strongly absorbs the following incident laser light, rapidly expands, and thereby sets in motion the remainder of the liquid droplet. We find an inverse-square dependence of this plasma-onset time on laser intensity and attribute this scaling to the presence of one-dimensional heat diffusion during irradiation. This scaling and its one-dimensional thermal origin is strongly established in literature and follows from a square-root scaling of the thermal diffusion depth with time. Our experiment unambiguously shows that this scaling law holds for our specific case of nanosecond laser impact on tin microdroplets. The results presented in this work are of particular interest to target preparation and metrology in extreme-ultraviolet sources utilizing tin microdroplet targets.

Keywords Ablation · Tin · Reflection

1 Introduction

Pulsed laser ablation of metals using laser pulses with durations in the nanosecond regime is of interest to a wide range of applications such as micromachining [1], pulsed laser deposition (PLD) [2], optical material design [3], and laser-induced breakdown spectroscopy (LIBS) [4]. A detailed understanding of laser ablation is also of value within the context of extreme-ultraviolet (EUV) light sources used in state-of-the-art nanolithography devices. Such EUV sources make use of mass-limited tin-droplet targets in a multi-pulse scheme [5].

Although the ablation of liquid tin microdroplets is well understood in a steady-state regime above the plasma formation threshold [6], accurate modeling appears challenging close to the threshold [7], indicative of an incomplete understanding of this highly transient ablation regime. Experimental investigations into the ablation threshold and ablation mechanics may therefore be of value to advance our understanding of laser-droplet interaction, and be of significant benefit to EUV source development in the context of droplet deformation, debris mitigation, and metrology. Furthermore, accurate knowledge of ablation thresholds and an understanding of the possibility of phase explosion is valuable in the context of advanced target preparation, where laser vaporization of the liquid tin below the plasma formation threshold can possibly be used to generate low-density vapor targets [8].

We therefore study the laser ablation threshold of liquid tin microdroplets by making use of time-resolved measurements of the surface reflection. A strong and abrupt decrease in the reflection of temporally square (constant intensity) laser pulses from the droplet, indicates a moment of plasma onset and the coinciding inception of inverse bremsstrahlung absorption of the laser light by the plasma [6, 9, 10]. For near-infrared wavelengths, the time required for ionization,

✉ S. Witte
   s.witte@arcnl.nl

   R. A. Meijer
   r.meijer@arcnl.nl

1 Advanced Research Center for Nanolithography (ARCNL), Science Park 106, 1098 XG Amsterdam, The Netherlands

2 LaserLab, Department of Physics and Astronomy, Vrije Universiteit, De Boelelaan 1105, 1081 HV Amsterdam, The Netherlands

3 ASML Netherlands B.V., De Run 6501, 5504 DR Veldhoven, The Netherlands

due to electron acceleration by the laser field and subsequent electron atom collisions, is typically on the order of 100 ps [11]. Subsequently, the transition from atomic vapor to plasma rapidly occurs within single nanoseconds by an electron avalanche process. For nanosecond-duration pulses, this then results in an apparent coincidence of the vapor and plasma formation thresholds, hence the ablation threshold under consideration is that of plasma formation. Accordingly, we here study the moment of plasma formation as a function of laser pulse duration and energy, and correlate the reflection signal with target deformation recorded using shadowgraphy imaging.

2 Experiment and methods

A schematic illustration of the experiment is depicted in Fig. 1. We irradiate the tin microdroplets (99.995% purity), 30 μm in diameter, in a vacuum environment with circularly polarized pulses from an Nd:YAG laser system. The in-house-built laser system [12], operating at 1064 nm wavelength, is programmed to output flat-intensity pulses with a duration ranging from 100 to 400 ns and rise times of approximately 200 ps. The laser beam with a diameter of 6 mm is focused down ($f = 500$ mm) to a Gaussian focal spot with a full width at half maximum (FWHM) of 84 μm at the location of the droplet. The laser fluence employed in this work ranges from approximately 0.7 J/cm^2 for a 100 ns pulse to 7.5 J/cm^2 for a 200 ns pulse.

A photodiode (PD, Thorlabs DET08) is mounted on the vacuum chamber at a 21° angle with respect to the principal laser axis and detects the laser light reflected from the droplet. The photodiode signal V_{PD} is recorded using a 1-GHz-bandwidth oscilloscope set to a 50 Ω input impedance. To increase the signal on the PD and block any broadband emission from the plasma, a lens and laser-line filter are mounted ahead of the PD, respectively. Since V_{PD} ranges from approximately 100 μV to a few mV, 720 pulses are recorded and averaged to improve the signal-to-noise ratio.

The droplets are imaged using a shadowgraphy system aligned perpendicularly to the principal laser axis, providing a side view. The system consists of a CCD camera coupled to a long-distance microscope, and makes use of incoherent-pulsed backlighting with a wavelength of 560 nm. We obtain a spatial and temporal resolution of approximately 5 μm and 5 ns respectively. More information on the experimental setup can be found in Refs. [7, 13, 14].

3 Results

3.1 Time-resolved reflection and its correlation with deformation

Figure 2 shows the time-resolved reflection signals obtained for the case of a 400 ns laser pulse with energies E_L ranging from 1 to 6.3 mJ. For all energies, the reflection from the droplet initially accurately follows the flat input pulse. At a certain point in time the reflection starts to deviate, displaying a strong decrease for all values of E_L except the lowest two, for which only a gradual increase in reflected light is observed. We attribute the decrease in reflectivity to the generation of a plasma layer that efficiently absorbs the incident laser light [9] and therefore label the moment at which this occurs as the plasma-onset time t_{on}. Several studies [15–17] on the reflection of nanosecond laser pulses in ablation of metals have attributed a similar observation of decreased reflectivity to the absorption of the laser light in plasma. Furthermore, in agreement with our observation, Refs. [15–17]
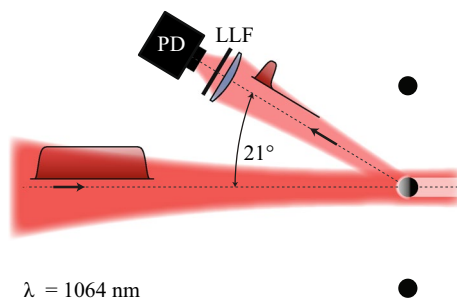

Fig. 1 Illustration of the experiment. A temporally flat, constant-intensity pulse is incident on the tin droplet which is positioned in the focus of the laser beam. The reflected laser light is detected by a photodiode (PD, Thorlabs DET08) at 21° with respect to the principal laser axis. Upstream from the photodiode a lens is used to increase the total light collection, and a 1064 nm laser-line filter (LLF) blocks the broadband plasma emission
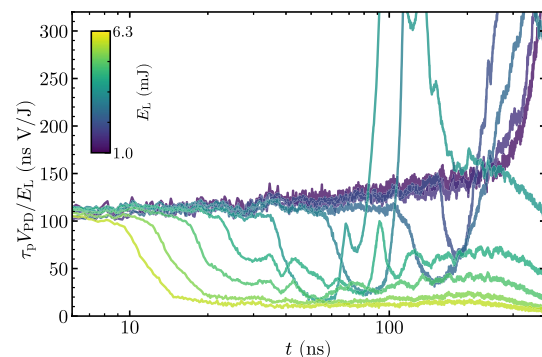

Fig. 2 Reflection signal as a function of time t from a 400-ns-flat-intensity pulse of varying laser pulse energy E_L incident on the droplet. The output voltage of the photodiode V_{PD} is normalized by the laser intensity E_L / τ_p

show no significant change in reflectivity before the plasma-formation threshold is reached.

After the initial decrease ($t > t_{on}$) the majority of the measurements show an increase in reflection. This increase appears to be caused by a hydrodynamic deformation of the droplet initiated by the rapidly expanding plasma [13]. In Fig. 3, shadowgrams of the droplet are compared to the reflection signal for the case of a 200 ns pulse. We observe a clear correlation between the decrease in reflection intensity and the first observable deformation which reproducibly originates from the droplet pole. This deformation is significant during the remainder of the laser pulse and influences the observed reflection signal. When plasma generation is minimal it is very likely that the deformed surface will occasionally, with a significant shot-to-shot deviation, direct additional light towards the photodiode. We also observe that the increased reflection at times $t > t_{on}$ is highly irregular (see also Fig. 2), which also hints at it originating from the somewhat volatile deformation. When E_L is increased, the increase in reflection following t_{on} is suppressed and reflection remains low (for example for the maximum E_L case in Fig. 2, 6.3 mJ). In these cases, plasma emission also largely or fully obscures local deformation on the shadowgraphy images (not shown). Both observations hint towards a full shielding of the droplet surface by the plasma. Note that no EUV emission takes place under these conditions as it requires higher laser intensities ranging from 10^{10} to 10^{11} W/cm^2 [18]. In Appx. A we present a brief quantification of the reduction in reflectivity in the full plasma shielding case alongside extra detail of the chaotic behavior of the reflection in the non-fully shielded case.

The observation that the deformation originates at the droplet pole, which therefore also marks the location of first plasma-onset, is expected. The effective laser intensity per droplet surface rapidly drops off with increasing incidence angle. This drop off is mostly due to the "Lambert" cosine projection of the beam onto the droplet surface. To a lesser extent, it is caused by the Gaussian shape of the focal spot. Furthermore, the Fresnel absorption coefficient decreases with increasing angle of incidence up to approximately 60° for circularly (equivalently: unpolarized) laser light. The fact that our PD detection angle at 21° is not strictly orthogonal to the beam propagation direction, combined with the observation that the plasma onset occurs at the droplet pole could be responsible for the lack of a decrease in reflection signal for the lowest values of E_L if plasma generation is only local.

3.2 Dependence of the plasma-onset time on laser intensity

The plasma-onset time t_{on} is quantified by fitting a Gaussian distribution to the gradient of the reflection drop. This provides an accurate center value of t_{on} as well as a standard-deviation width which we take to represent the measurement accuracy. Since the observed deformation following plasma
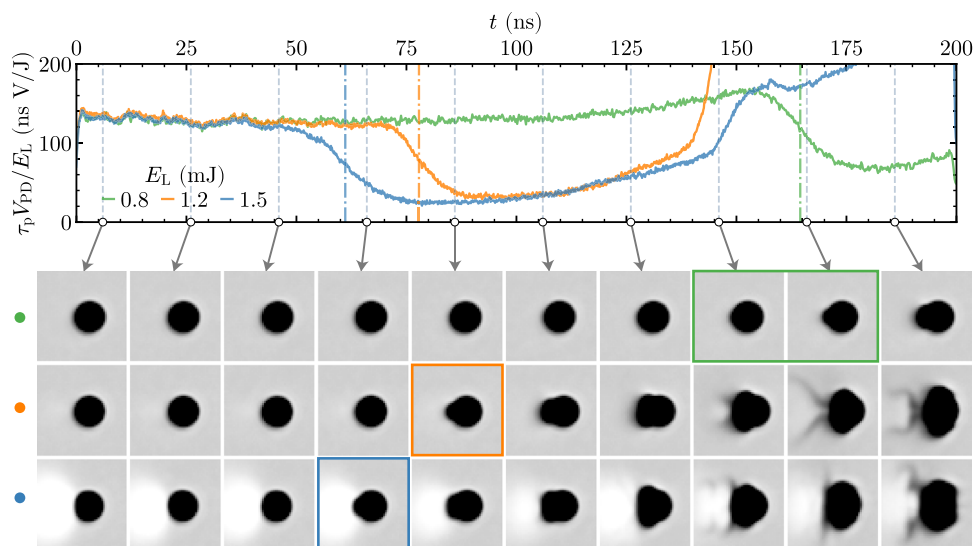

Fig. 3 Comparison between the obtained reflection signal (top) and the side-view shadowgraphy images (bottom) for three cases of laser pulse energy E_L and duration $\tau_p = 200$ ns. The rows of shadowgraphy images are ordered with increasing energy from top to bottom. The first observable deformation for each row is indicated by the outlined image(s). The determined t_{on} (at 50% of the decrease in $\tau_p V_{PD}/E_L$) is indicated by the vertical dash-dotted lines. For the 1.5 mJ case (bottom row) clear overexposure of the camera by emission from the plasma cloud is visible. Due to the relatively long exposure time of the camera (on the order of milliseconds) this emission is recorded in all frames and thus not temporally resolved. The laser pulse is incident from the left, the droplet diameter is 30 μm, and the figures are approximately 100 by 100 μm

onset originates on the droplet pole, we take as the relevant laser intensity I the peak value on the droplet pole. We determine I using a camera recording of the focal spot and the laser pulse energy E_L. The resulting dependency of t_{on} on I is presented in Fig. 4(a) for all pulse durations studied in this work. We observe a clear inverse-square dependence and therefore write

$$t_{on} = K_I I^{-2}. \tag{1}$$

A least-squares fit of Eq. (1) to the full dataset, with the error in t_{on} taken as weights, results in $K_I = 3.40(5) \times 10^8$ s W^2/cm^4. To obtain an absolute accuracy we need to include the typical 5% calibration error in the laser intensity measurement (indicated by the horizontal error bars) resulting in $K_I = 3.4(4) \times 10^8$ s W^2/cm^4. Note that three extra data points, recorded with a larger droplet size of 40 μm, are in full agreement with the data taken with 30 μm droplets. This agreement indicates no significant contribution of the droplet size on the observed intensity dependence (Eq. (1)) in the here studied range.

The two pulses with the lowest intensities studied in this work are the lowest energy cases with a 400 ns duration. For those two cases, we only observe a gradual increase in reflection at the end of the pulse, and no decrease as shown in Fig. 2. Regardless of the precise details of the ablation process in this regime and the existence of an equivalent t_{on}, since we observe no decrease we cannot determine a value for t_{on} in a similar fashion. Therefore, we have indicated the
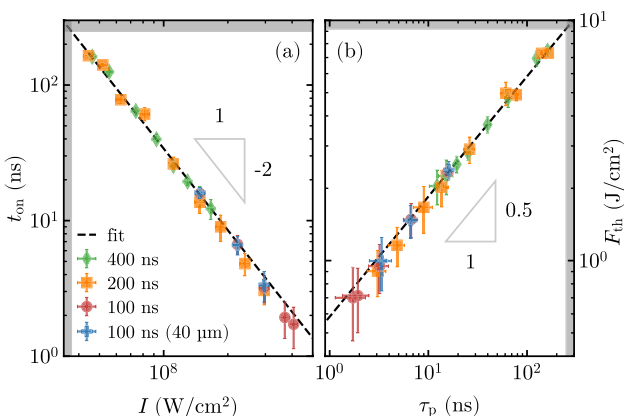
bounds of this regime in Fig. 4 with the grey shaded regions, and consider it out of reach with our current method.

Early work [19] on the heating and evaporation of strongly absorbing media by laser irradiation predicted the scaling relation given by Eq. (1), using the following argument: since the pulse duration is much longer than the electron-ion relaxation time, i.e., $\tau_p \gg \tau_{e-i}$, the electrons and ions in the liquid are in thermodynamic equilibrium and we can consider a gradual surface heating of the material by the incident laser pulse [20]. Assuming one-dimensional heat diffusion, the energy deposited through absorption of laser radiation AIt, with A the absorption coefficient, is distributed in a layer of thickness l, which grows following [21]

$$l \propto \sqrt{\kappa t}, \tag{2}$$

with κ the thermal diffusivity. Any threshold related to exceeding a certain specific internal energy in the material, given by AIt_{th}/l, is therefore reached at a time $t_{th} \propto I^{-2}$ [22].

The agreement between the above and the observed scaling following Eq. (1) indicates a (close-to) one-dimensional diffusion of heat in our case, also supported by the equal result for 30 and 40 μm droplets. Since we are not dealing with a planar target but a spherical droplet, the assumption of one-dimensional heat diffusion firstly only holds if the thermal penetration depth remains significantly smaller than the droplet size. Indeed, for a pulse duration of 100 ns and a thermal diffusivity of 16.4 mm^2/s [23], we estimate a thermal penetration depth of $l_{100} = \sqrt{\kappa \times 100 \, \text{ns}} \approx 1.3 \, \mu\text{m} \ll 30 \, \mu\text{m}$. However, as discussed previously plasma onset occurs on the droplet pole. In this case the agreement with one-dimensional heat diffusion suggests that a region significantly larger than the thermal penetration depth is uniformly heated. This means that although it is localized to the droplet pole, heating of the droplet surface is similar over an area with a radius of possibly several micrometers. Since the "Lambert" cosine projection on the droplet surface is the dominant mechanism of the reduction of laser intensity at increased angle of incidence, the laser intensity will have decreased by approximately 10% at a 26° angle of incidence. This corresponds to a total arc length of 13.5 μm, much larger than the 1.3 μm estimate of the thermal penetration depth, which likewise supports the notion that heat diffusion takes place in a one-dimensional fashion.

3.3 Fluence ablation threshold scaling with pulse duration

The observed scaling of $t_{on} \propto I^{-2}$ is essentially equivalent to a more commonly studied scaling of the fluence damage threshold F_{th} with pulse duration τ_p. Since $F_{th} = It_{on}$ for a pulse with a duration equal to the plasma-onset time, i.e. $\tau_p = t_{on}$, we obtain

Fig. 4 (**a**) plasma-onset time t_{on} as function of laser intensity I. Dashed line is a fit of Eq. (1) to the concatenated data. The different symbols and colors represent laser pulses of different duration as labeled in the legend. (**b**) Ablation fluence threshold F_{th} as function of synthetic pulse duration $\tau_p = t_{on}$. Here, the dashed line follows Eq. (4) with K_I obtained from the fit of Eq. (1) as shown in (a). Several data points were taken at an alternate droplet size of 40 μm and are labeled as such in the legend. The grey shaded regions indicate the edge of the parameter space in reach with our current reflection-based method (see main text)

$$F_{th} = \sqrt{K_I \tau_p}. \tag{3}$$

This relation is applied to the data and previous fit result, and plotted in Fig. 4(b). With $K_I = 3.4(4) \times 10^8 \, s \, W^2/cm^4$ obtained previously, the corresponding proportionality constant has a value of $\sqrt{K_I} = 1.84(10) \times 10^4 \, J \, cm^{-2} \, s^{-1/2}$. The square-root dependence of the threshold fluence on the pulse duration (Eq. (3)) again directly follows from the same form of the thermal penetration depth (Eq. (2)). For the case of laser-induced damage in dielectrics the square-root scaling is also well established and confirmed to hold for pulse durations down to approximately 10 ps [24–28].

In Ref. [13], a value of $F_{th,10} = 2.4(8) \, J \, cm^{-2}$ was obtained from an independent measurement of the droplet propulsion threshold for the case of a 10 ns FWHM Gaussian pulse. Using the here obtained value of $\sqrt{K_I}$ we get $F_{th,10} = \sqrt{K_I \times 10^{-8}} = 1.84(10) \, J \, cm^{-2}$, which is in good agreement with the threshold obtained from propulsion. The propulsion of tin microdroplets resulting from laser impact has been further studied in detail in several other works [7, 29], which have confirmed the above propulsion threshold and include quantitative analyses of the ablation pressure employing both experiment and modeling.

As stated previously, for nanosecond laser ablation using near-infrared wavelengths, a near equivalence of vapor and plasma formation thresholds is typically observed [11, 30]. Accordingly, a value for F_{th} is commonly estimated by considering a threshold of strong evaporation. Such a threshold can be expected to be passed when the deposited energy per unit mass ε exceeds the latent heat of evaporation $\varepsilon > \Delta H$. Here, the initial state (solid or liquid) and temperature of the material are typically ignored, as the latent heat of fusion and the energy required to heat the material to the vaporization temperature are much smaller than ΔH. The fluence threshold can then be written as [22, 31, 32]

$$F_{th} = A^{-1} \rho_0 \Delta H \sqrt{\kappa \tau_p}, \tag{4}$$

with absorption coefficient A, density ρ_0, latent heat of vaporization ΔH, and thermal diffusivity κ.

Before the onset of plasma formation, absorption through inverse bremsstrahlung is negligible and we can estimate the absorption of liquid tin given its optical constants [33] and obtain $A = 0.16$ for the relevant wavelength of 1064 nm. With literature values for the various constants, $\rho_0 = 7 \times 10^3 \, kg \, m^3$ [34], $\Delta H = 2.5 \times 10^6 \, J \, kg^{-1}$ [35], and $\kappa = 16.4 \, mm^2/s$, we obtain $A^{-1} \rho_0 \Delta H \sqrt{\kappa} = 4.4 \times 10^4 \, J \, cm^{-2} \, s^{-1/2}$. This value can be directly compared with our value of $\sqrt{K_I}$ obtained from the fit to the data and, given the simplicity of this estimate comes remarkably close. The present discrepancy could indicate that either Eq. (4) does not fully accurately describe the ablation process and the observed threshold in our experiment, or that one or multiple of the constants (ρ_0, κ, ΔH, and the refractive index) available in literature are inaccurate or exhibit a significant temperature dependence.

3.4 On alternative explanations for the loss of reflection

In our interpretation of the results, we have assumed that the drop in reflectivity arises due to the strong absorption of the laser light in plasma by inverse bremsstrahlung. Although this assumption was made with fair support, including our experimental observation of plasma emission, it is valuable to discuss alternative explanations. Here we briefly discuss and exclude other mechanisms that could hypothetically contribute to the reduction of reflectivity without plasma formation.

First, we consider the occlusion of the droplet surface by a formed cloud of atoms. Such a cloud will not strongly interact with the incident laser light unless the frequency of the light overlaps with an atomic transition. No such transition is known to exist for the incident laser wavelength of 1064 nm. We can therefore exclude that the formation of a cloud of atoms shields the droplet surface from the laser pulse and contributes significantly to a loss in reflection.

Second, we consider a modification of the droplet surface, which, since the target is liquid, would entail a hydrodynamic deformation. However, hydrodynamic deformation of the droplet takes place on a capillary timescale ($\sim 10 \, \mu s$) [36], many times larger than typical timescale of the loss of reflection (~ 10. Undoubtedly, an initial hydrodynamic deformation can take place in a fraction of the capillary time, as can be seen in the shadowgraphy measurements of Fig. 3, but a rapid modification of the droplet surface seems unlikely and is not able to explain the abrupt decrease in reflectivity on a time scale of 1 ns to 10 ns.

Scattering and absorption by nanodroplets, either expelled from the droplet or formed in the expanding vapor plume prior to plasma formation is another possibility. We consider it highly unlikely that particles form at a sufficient quantity to significantly contribute to the observed loss of reflection. Regardless, we can exclude this mechanism on the basis of the shadowgraphy measurements shown in Fig. 3. Tin nanodroplets of any size will scatter or absorb more strongly at the 560-nm wavelength of our shadowgraphy illumination and be visible. Since on our shadowgraphy images we simply do not see such nanodroplets leaving the target, we can exclude such a mechanism. Note, that following the threshold moment we do see a peculiar bubble formation in the shadowgraphy, followed by dark streaks indicative of nanodroplets. This observation is discussed next.

3.5 On the presence of phase explosion

The deformation as shown in Fig. 3 shows the peculiar formation of an expanding bubble-like feature on the droplet pole. The bubble grows over time and eventually appears to burst, followed by low-contrast 'streaks' indicative of a plume containing particles with sizes far below the imaging resolution of 5 μm. These observations hint at a (subsurface) phase explosion (PE) taking place as a result of a superheating of the liquid metal to a temperature approaching the critical temperature [37–40]. In the lowest energy case of 0.8 mJ shown in Fig. 3 we observe a slight gradual increase in reflection and a significant bulging of the droplet surface before t_{on}. This suggests that PE might take place at a threshold time slightly preceding the onset of plasma formation t_{on} and the subsequent absorption of laser light due to inverse bremsstrahlung. An opposite order of the thresholds is unlikely as a plasma shielding effect [38, 41–43] will decrease the rate at which the droplet surface is heated by the laser pulse, thereby preventing PE from occurring. Further investigation into the presence of PE in our experiment and a possible PE threshold separate from that of plasma formation is outside the scope of this work. Such investigations would likely require additional measurements using shadowgraphy with an increased spatial resolution, possibly assisted by shadowgraphy at shorter (UV) wavelengths to improve vapor contrast, (time-of-flight) ion diagnostics [44], and time-resolved recordings and spectroscopic investigation of the plasma emission [45, 46]. Future work could confirm the possibility of applying PE as a distinct new way of initiating droplet deformation.

4 Conclusions

In this work, we have determined the laser ablation, i.e., plasma formation threshold using measurements of the time-resolved reflection from temporally flat near-infrared nanosecond laser pulses incident on tin microdroplets. The reflection exhibits strong drops at the moment of plasma formation due to the strong absorption of the laser light by the inverse-bremsstrahlung mechanism. The drop in reflection is as such well correlated with the initiation of deformation of the liquid droplet as observed with shadowgraphy. We found that the observed moment of plasma formation exhibits a well-established inverse-square dependence with laser intensity, which follows from a one-dimensional diffusion of heat from the absorbing droplet surface into the droplet interior. We have quantified this threshold over an order of magnitude of laser intensities spanning from 4×10^7 to 4×10^8 W/cm^2 and for pulse durations up to 400 ns. Furthermore, we found excellent agreement with a previously determined ablation threshold based on droplet propulsion and provide an almost

ten times improvement on the accuracy. A comparison of our obtained threshold values with a commonly used, straightforward model of strong evaporation reveals some discrepancy, supplying motivation for future investigation and modeling efforts. Our obtained value of the nanosecond laser ablation threshold on tin microdroplets are of direct use within the scopes of target preparation and metrology in extreme-ultraviolet sources.

By making use of a "pre-pulse" to deform a droplet into a thin sheet [13, 47], studying the ablation of (free-falling) liquid-metal thin films is within experimental reach. As shown, the inverse-square scaling of the ablation threshold with laser intensity as presented in Sec 3.2 arises from the presence of one-dimensional thermal diffusion. In the thin-film limit such thermal diffusion is absent, entering a regime of thermal confinement accompanied by changes in ablation thresholds [48]. The current work could be extended by measuring the transition between bulk and thin-film ablation regimes, utilizing the sheet thinning over time resulting from pre-pulse impact [47]. Plasma shielding is likely undesired in an advanced EUV-source vapor-target preparation scheme [8] as it prevents vaporization of part of the liquid mass and possibly disturbs the formation of a uniform "cloud" target. By measuring the plasma onset thresholds for the case of thin sheets, we can therefore identify a parameter range possibly beneficial to target preparation for droplet-based EUV sources.

Appendix A Brief analysis of reflection following plasma onset

Extra characterization of the reflection after the plasma onset threshold is passed is presented in Fig. 5. We simplify the observed behaviour into two cases, partial and full plasma shielding of the droplet. In the partially shielded case, averaging of the reflection signal obtained from many laser shots obscures the original chaotic behavior. Therefore, in Fig. 5(a) several single acquisitions are compared to the average of all 720 measurements. All traces coincide up until, and also slightly after, the drop in reflection attributed to the plasma generation. At later times, the plasma recoil pressure initializes deformation and a disorganized reflection signal consisting of many randomized peaks strongly differs from shot to shot.

In Figure 5(b) we show a quantification of the decrease of reflection when the droplet is fully shielded by the plasma cloud. A background signal is taken by misaligning the droplet to laser timing such that the droplet is missed. By subtraction of this background signal we find a remaining reflection of only 0.3% with a signal-to-noise ratio of 1.7, in line with expectations of strong inverse bremsstrahlung absorption in dense plasmas.
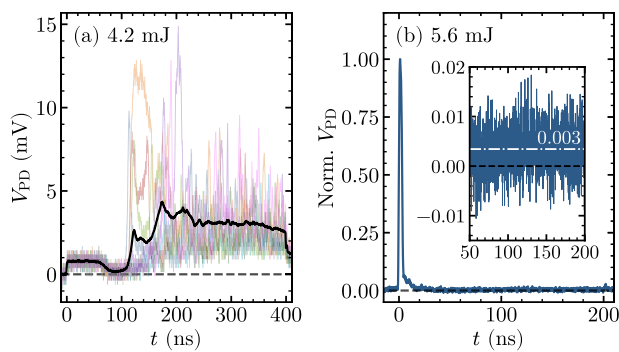
Fig. 5 (**a**) Average (black) of 720 events overlaid on a selection (n=7) of single events illustrates the chaotic behavior of the reflection following plasma formation. (**b**) Reflection of a 5.6 mJ, 200 ns pulse for which the plasma fully shields the droplet

Availability of data and material The data that support the findings of this study are available from the corresponding author upon reasonable request.

Code availability The analysis code that used in this study is available from the corresponding author upon reasonable request.

Declarations

Conflict of interest The authors declare that they have no conflict of interest.

References

1. S. Mishra, V. Yadava, Opt. Lasers Eng. **73**, 89 (2015)
2. P.R. Willmott, J.R. Huber, Rev. Mod. Phys. **72**(1), 315 (2000)
3. A.J. Glass, A.H. Guenther, In: Boulder damage symposium, (1976)
4. D.W. Hahn, N. Omenetto, Appl. Spectrosc. **66**(4), 347 (2012)
5. I.V. Fomenkov, A.A. Schafgans, D.C. Brandt, Synchrotron Radiat. News **32**(4), 3 (2019)
6. M.M. Basko, V.G. Novikov, A.S. Grushin, Phys. Plasmas **22**(5), 053111 (2015)
7. D. Kurilovich, M.M. Basko, D.A. Kim, F. Torretti, R. Schupp, J.C. Visschers, J. Scheers, R. Hoekstra, W. Ubachs, O.O. Versolato, Phys. Plasmas **25**(1), 012709 (2018)
8. B. Liu, R.A. Meijer, J. Hernandez-Rueda, D. Kurilovich, Z. Mazzotta, S. Witte, O.O. Versolato, J. Appl. Phys. **129**, 053302 (2021)
9. P. Mora, Phys. Fluids **25**(6), 1051 (1982)
10. O.O. Versolato, Plasma Sour. Sci. Technol. **28**(8), 083001 (2019)
11. E.G. Gamaly, A.V. Rode, B. Luther-Davies, Appl. Phys. A Mater. Sci. Process. **69**(7), 121 (1999)
12. R.A. Meijer, A.S. Stodolna, K.S.E. Eikema, S. Witte, Opt. Lett. **42**(14), 2758 (2017)
13. D. Kurilovich, A.L. Klein, F. Torretti, A. Lassise, R. Hoekstra, W. Ubachs, H. Gelderblom, O.O. Versolato, Phys. Rev. Appl. **6**(1), 014018 (2016)
14. D. Kurilovich, Laser-induced dynamics of liquid tin microdroplets. Ph.D. thesis, Vrije Universiteit Amsterdam (2019)
15. O. Benavides, O. Lebedeva, V. Golikov, Opt. Express **19**(22), 21842 (2011)
16. O. Benavides, L.d.l.C. May, A.F. Gil, Optics Express **21**(11), 13068 (2013)
17. O. Benavides, L. De La Cruz May, A. Flores Gil, J.A. Lugo Jimenez, Optics Laser Eng **68**, 83 (2015)
18. R. Schupp, F. Torretti, R.A. Meijer, M. Bayraktar, J. Scheers, D. Kurilovich, A. Bayerle, K.S.E. Eikema, S. Witte, W. Ubachs, R. Hoekstra, O.O. Versolato, Phys. Rev. Appl. **12**(1), 014010 (2019)
19. Y.V. Afanasyev, O.N. Krokhin, G.V. Sklizkov, IEEE J. Quantum Electron. **2**(9), 483 (1966)
20. H.M.J. Musal, In: Laser induced damage in optical materials (1979), pp. 159–173
21. A. Faghri, Y. Zhang, In: Transport phenomena in multiphase systems (2006), chap. 1, pp. 1–106
22. B.N. Chichkov, C. Momma, S. Nolte, F. von Alvensleben, A. Tünnermann, Appl. Phys. A Mater. Sci. Proces. **63**, 109 (1996)
23. I.V. Savchenko, S.V. Stankus, A.S. Agadjanov, High Temp. **49**(4), 506 (2011)
24. J.R. Bettis, R.A.I. House, A.H. Guenther, In: Laser induced damage in optical materials (1976)
25. D. Du, X. Liu, G. Korn, J. Squier, G. Mourou, Appl. Phys. Lett. **64**(23), 3071 (1994)
26. B.C. Stuart, M.D. Feit, A.M. Rubenchik, B. Shore, M.D. Perry, Phys. Rev. Lett. **74**(12), 2248 (1995)
27. B.C. Stuart, M.D. Feit, S. Herman, A.M. Rubenchik, B. Shore, M. Perry, Phys. Rev. B Condens. Matter Mater. Phys. **53**(4), 1749 (1996)
28. A.C. Tien, S. Backus, H. Kapteyn, M.M. Murnane, G. Mourou, Phys. Rev. Lett. **82**(19), 3883 (1999)
29. J. Hernandez-Rueda, B. Liu, D.J. Hemminga, Y. Mostafa, R.A. Meijer, D. Kurilovich, H. Gelderblom, J. Sheil, O.O. Versolato, Phys. Rev. Res. **013142**(4), 1 (2022)
30. M.S. Qaisar, G.J. Pert, J. Appl. Phys. **94**(3), 1468 (2003)
31. M. Aden, E. Beyer, G. Herziger, H. Kunze, J. Phys. D Appl. Phys. **25**(1), 57 (1992)
32. E.G. Gamaly, A.V. Rode, B. Luther-Davies, V.T. Tikhonchuk, Phys. Plasmas **9**(3), 949 (2002)
33. G. Cisneros, J.S. Helman, C.N. Wagner, Phys. Rev. B **25**(6), 4248 (1982)
34. M.J. Assael, A.E. Kalyva, K.D. Antoniadis, R. Michael Banish, I. Egry, J. Wu, E. Kaschnitz, W.A. Wakeham, J. Phys. Chem. Ref. Data **39**(3), 033105 (2010)
35. S. Sharafat, N. Ghoniem, *Summary of Thermo-Physical Properties of Sn, And Compounds of Sn-H, Sn-O, Sn-C, Sn-Li, and Sn-Si, And Comparison of Properties of Sn, Sn-Li, Li, and Pb-Li* (University of California Los Angeles, Tech. rep., 2000)

36. H. Gelderblom, H. Lhuissier, A.L. Klein, W. Bouwhuis, D. Lohse, E. Villermaux, J.H. Snoeijer, J. Fluid Mech. **794**, 676 (2016)
37. A. Miotello, R. Kelly, Appl. Phys. Lett. **67**, 3535 (1995)
38. Q. Lu, Physical Review E - Statistical Physics. Plasmas, Fluids, and Related Interdisciplinary Topics **67**(1), 5 (2003)
39. C. Porneala, D.A. Willis, Int. J. Heat Mass Transf. **49**(11–12), 1928 (2006)
40. C. Porneala, D.A. Willis, Appl. Phys. Lett. **89**(21), 211121 (2006)
41. L. Balazs, R. Gijbels, A. Vertes, Anal. Chem. **63**(4), 314 (1991)
42. D. Marla, U.V. Bhandarkar, S.S. Joshi, J. Appl. Phys. **109**(2), 021101 (2011)
43. D. Autrique, G. Clair, D. L'Hermite, V. Alexiades, A. Bogaerts, B. Rethfeld, J. Appl. Phys. **114**(2), 023301 (2013)
44. A. Bayerle, M.J. Deuzeman, S. van der Heijden, D. Kurilovich, Td.F. Pinto, A.S. Stodolna, S. Witte, K.S.E. Eikema, W. Ubachs, R. Hoekstra, O.O. Versolato, Plasma Sour. Sci. Technol. **27**(4), 045001 (2017)
45. J. Scheers, R. Schupp, R.A. Meijer, W. Ubachs, R. Hoekstra, O.O. Versolato, Phys. Rev. E **102**(1), 13204 (2020)
46. F. Torretti, R. Schupp, D. Kurilovich, A. Bayerle, J. Scheers, W. Ubachs, R. Hoekstra, O.O. Versolato, J. Phys. B **51**(4), 045005 (2018)
47. B. Liu, D. Kurilovich, H. Gelderblom, O.O. Versolato, Phys. Rev. Appl. **13**(2), 024035 (2020)
48. A.H. Lutey, J. Appl. Phys. **114**(8), 083108 (2013)